

Boltzmann approach to collective motion via non-local visual interaction

Susumu Ito and Nariya Uchida*

Department of Physics, Tohoku University, Sendai, 980-8578, Japan

(Dated: August 30, 2024)

Visual cues play crucial roles in the collective motion of animals, birds, fish, and insects. The interaction mediated by visual information is essentially non-local and has many-body nature due to occlusion, which poses a challenging problem in modeling the emergent collective behavior. In this Letter, we introduce a Boltzmann-equation approach incorporating non-local visual interaction. Occlusion is treated in a self-consistent manner via a coarse-grained density field, which renders the interaction effectively pairwise. Our model also incorporates the recent finding that each organism stochastically selects a neighbor to interact at each instant. We analytically derive the order-disorder transition point, and show that the visual screening effect substantially raises the transition threshold, which does not vanish when the density of the agents or the range of the intrinsic interaction is taken to infinity. Our analysis suggests that the model exhibits a discontinuous transition as in the local interaction models, and but the discontinuity is weakened by the non-locality. Our study clarifies the essential role of non-locality in the visual interactions among moving organisms.

Collective motion is ubiquitously found in Nature [1]. Visual information plays an important role in the interaction between organisms that have eyes: insects [2], fish [2, 3], birds [4], and humans [5]. In the visual interaction, each organism often selects a specific neighbor to interact with and decides its next motion [2, 5, 6]. The selective decision-making reduces the load on the information processing system in the brain [7]. A recent study proposes a mechanism of stochastic pairwise interaction, in which each individual randomly selects another and copy its orientation [8].

Agent-based models are a powerful tool to simulate collective motion [9–11]. Some of them consider visual information under the assumption that each agent interacts with all detected neighbors simultaneously [4, 12–15]. Several other models incorporate selective decision-making, and reproduce experimental results for specific organisms [2, 5, 16–18].

Continuum description has also been used to elucidate the nature of phase transitions in conventional models of collective motion [19–24]. In particular, the Boltzmann approach, which describes time evolution of a probability distribution function by pairwise collision and alignment of agents, is successfully used to derive hydrodynamic equations and analyze phase transition [21–24]. However, fundamental aspects of phase transition arising from visual interaction is not yet clear. The difficulty lies in the many-body nature of occlusion, where the interaction between two individuals is screened by the other individuals in between.

In this Letter, we introduce a Boltzmann approach to collective motion induced by non-local visual interaction. Motivated by the experimental finding [8], we assume that an agent randomly selects a distant neighbor and one at a time, which has good affinity with the framework of the Boltzmann equation. We incorporate occlusion by coarse-graining the clouds of intervening agents as a density field, which is self-consistently determined by the

Boltzmann equation. This results in an effective pairwise interaction between agents. In the absence of occlusion, the probability to select a neighbor decays with a characteristic distance determined by the resolution of the eye system. We analytically derive the order-disorder transition point, and show that it is substantially shifted by the visual screening effect. Furthermore, we find that the non-locality of interaction suppresses the discontinuity of the phase transition in comparison to local collision models [21, 25], and that the polar order parameter exhibits a mean-field critical behavior in the weak-advection limit and in a finite system.

Model.— We consider a two-dimensional model where each agent is described by its position $\mathbf{r} = (x, y)$ and direction of motion $\mathbf{e}(\theta) = (\cos \theta, \sin \theta)$. For simplicity, we assume that each agent moves with a constant speed v_0 and its shape is a circle of diameter D (see Fig. 1). We define the probability distribution function $f(\mathbf{r}, \theta, t)$ and the number density of agents $\rho(\mathbf{r}, t) = \int_{-\pi}^{\pi} d\theta f(\mathbf{r}, \theta, t)$. The Boltzmann equation describes time evolution of f

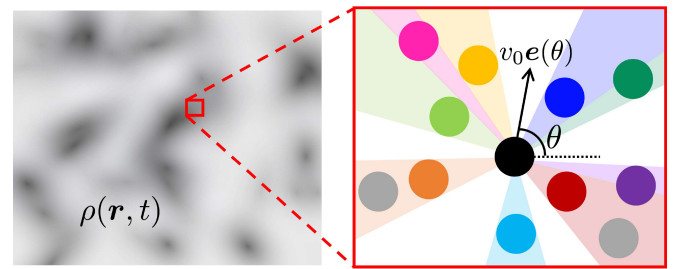


FIG. 1. Schematic illustration of the model. The left panel shows the clouds of agents described by the density field $\rho(\mathbf{r}, t)$ in the continuum description, and the right panel shows the discrete picture. Each agent has a circular shape and moving with the velocity $v_0 \mathbf{e}(\theta)$. The center agent (black) perceives the neighbors and interacts with one of them at a time. The agents shown in gray are not seen by the black agent due to occlusion.

via the self-diffusion term $I_{\text{self}}[f]$ and visual interaction term $I_{\text{vis}}[f]$ as follows:

$$\frac{\partial f}{\partial t} + v_0 \mathbf{e}(\theta) \cdot \nabla f = I_{\text{self}}[f] + I_{\text{vis}}[f], \quad (1)$$

$$I_{\text{vis}}[f] = -c \int d^2 \mathbf{r}' \int_{-\pi}^{\pi} d\theta' G(\mathbf{r}, \mathbf{r}' - \mathbf{r}, t) \Gamma(|\mathbf{r}' - \mathbf{r}|, \theta' - \theta) f(\mathbf{r}, \theta, t) f(\mathbf{r}', \theta', t) \quad (3)$$

$$+ c \int d^2 \mathbf{r}' \int_{-\pi}^{\pi} d\theta_1 \int_{-\pi}^{\pi} d\theta_2 G(\mathbf{r}, \mathbf{r}' - \mathbf{r}, t) \Gamma(|\mathbf{r}' - \mathbf{r}|, \theta_2 - \theta_1) f(\mathbf{r}, \theta_1, t) f(\mathbf{r}', \theta_2, t) \hat{p}(\theta - \vartheta(\theta_1, \theta_2)).$$

In the self-diffusion integral (Eq. (2)), s is the rate of reorientation by the noise, and $p(\theta)$ is the probability distribution function of angle change: we use the von Mises distribution $p(\theta) = e^{\kappa \cos \theta} / (2\pi I_0(\kappa))$, where $I_n = I_{n=0,1,\dots}(\kappa)$ is the modified Bessel function of the first kind and κ is the sharpness parameter [16]. In Eq. (2), the first and second term on the right-hand side represents the probability of transition from θ to any angle and from θ' to θ , respectively.

The visual interaction integral (Eq. (3)) describes the pairwise orientational interaction between the agent at \mathbf{r} and a neighbor at \mathbf{r}' . The rate of interaction is determined by occlusion by other agents and the intrinsic mechanism of visual recognition. The latter decays with distance due to the resolution of eyes [26] and also depends on the relative direction of motion [27]. Therefore, we introduce the occlusion factor $G(\mathbf{r}, \mathbf{R}, t)$ and the intrinsic factor $\Gamma(|\mathbf{R}|, \psi)$ in the interaction kernel, where $\mathbf{R} = \mathbf{r}' - \mathbf{r}$ and $\psi = \theta' - \theta$ ($\psi = \theta_2 - \theta_1$) are the relative position and angle, respectively. We will formulate them in the following paragraphs. In Eq. (3), c is the reference interaction rate, and $\hat{p}(\theta) = e^{\hat{\kappa} \cos \theta} / (2\pi I_0(\hat{\kappa}))$ is the probability distribution function of angle change for interaction [28]. The first term on the right-hand side represents the outgoing event in which the agent at (\mathbf{r}, θ) interacts with the neighbor at (\mathbf{r}', θ') and is reoriented from θ to another angle. The second term represents the incoming event where the agent at (\mathbf{r}, θ_1) interacts with the neighbor at (\mathbf{r}', θ_2) and is reoriented to their average angle $\theta = \vartheta(\theta_1, \theta_2) = \arg(e^{i\theta_1} + e^{i\theta_2})$ [21].

Now we formulate the occlusion factor $G(\mathbf{r}, \mathbf{R}, t)$, which is a key feature of our model. The resolution of the eye is limited by the number of ganglion cells in the retina [26], and represented by the azimuthal resolution angle Φ in our two-dimensional model. Images of the other agents within the angle Φ centered around the line of sight, which has the direction $\hat{\mathbf{R}} = \mathbf{R}/R$, are not distinguished from each other. We define the angular width $\Phi_G(\mathbf{r}, \mathbf{R}, t)$ of the regions that are *not* occupied by the images of the other agents within the distance R and within the angle Φ . The occlusion factor $G(\mathbf{r}, \mathbf{R}, t)$ is

$$I_{\text{self}}[f] = -s f(\mathbf{r}, \theta, t) + s \int_{-\pi}^{\pi} d\theta' p(\theta - \theta') f(\mathbf{r}, \theta', t), \quad (2)$$

defined as the probability that a neighbor at $\mathbf{r} + \mathbf{R}$ is visible for the agent at \mathbf{r} . Therefore, it reads

$$G(\mathbf{r}, \mathbf{R}, t) = \frac{\Phi_G(\mathbf{r}, \mathbf{R}, t)}{\Phi} \leq 1. \quad (4)$$

As the distance is increased in a given direction $\hat{\mathbf{R}}$, more agents come into the line of sight and decrease $\Phi_G(\mathbf{r}, \mathbf{R}, t)$. Let $\sigma(\mathbf{r}, \mathbf{R}, t) dR$ be the fraction of the angular region occupied by the agents in the distance between R and $R + dR$ and within the angle Φ . Given that they are randomly distributed, the unoccupied angular region Φ_G is reduced by the same fraction. Thus we obtain the differential equation

$$\frac{\partial}{\partial R} \Phi_G(\mathbf{r}, \mathbf{R}, t) = -\sigma(\mathbf{r}, \mathbf{R}, t) \Phi_G(\mathbf{r}, \mathbf{R}, t). \quad (5)$$

The occupied fraction is related to the local density as

$$\sigma(\mathbf{r}, \mathbf{R}, t) = \mathcal{D}(R) \rho(\mathbf{r} + \mathbf{R}, t), \quad (6)$$

where $\mathcal{D}(R)$ is the averaged body length inside the angular bin Φ , and is identical to the agent diameter D in the limit $R \rightarrow \infty$. At short distances, an agent covers the whole angular width Φ and thus \mathcal{D} is given by the arc length $R\Phi$. The formula for intermediate distances is derived by straightforward geometric calculation [29], and gives

$$\mathcal{D}(R) = \begin{cases} R\Phi & [R < R_D], \\ R_D \Phi \left(2 - \frac{R_D}{R}\right) & [R > R_D], \end{cases} \quad (7)$$

where $R_D = D/(2\Phi)$.

The differential equation (5) is solved under the boundary condition $\Phi_G|_{R \rightarrow 0} = \Phi$. Substituting the solution into Eq.(4), we obtain

$$G(\mathbf{r}, \mathbf{R}, t) = \exp\left(-\int_0^R dR' \mathcal{D}(R') \rho(\mathbf{r} + \mathbf{R}', t)\right), \quad (8)$$

The occlusion factor (Eq. (8)) gives an effective pairwise interaction mediated by the density field ρ , which is determined by the Boltzmann equation in a self-consistent manner.

Note that the coarse-grained description requires that many neighbors are observed in the resolution angle Φ . For the mean density ρ_0 , a neighbor in the typical distance $R \sim 1/\sqrt{\rho_0\Phi}$ (note that the number of agents in the distance R and angle Φ is estimated by $n \sim \rho_0 R^2 \Phi/2$) occupies the angle $\sqrt{\rho_0\Phi}D$ in the field of view, which should be much smaller than Φ . Thus we obtain the condition $\rho_0 \ll \Phi/D^2$ for the density. Under this condition, $R \gg R_D$ is satisfied in Eq. (7) for most cases, and the occlusion factor G decays with the characteristic distance $R_{\text{occ}} = 1/(\rho_0 D) \gg R$ [30]. Since $\Phi \ll 1$, the above condition also ensures that the area fraction $A = \rho_0 \pi (D/2)^2$ is much smaller than unity, which is required for the excluded-volume interaction to be negligible.

The intrinsic factor takes the form $\Gamma(R, \psi) = B(R)K(\psi)$, where

$$B(R) = \exp\left(-\frac{R^2}{2R_0^2}\right) \quad (9)$$

and

$$K(\psi) = \sqrt{2}|\sin \psi|. \quad (10)$$

Here, R_0 is the characteristic distance for visual recognition [26, 27]. Eqs. (9),(10) mean that an agent easily responds to a neighbor within the distance R_0 and to a neighbor with the relative angle ψ close to $\pm\pi/2$ [31].

Results.— As we increase the interaction rate c , the uniform disordered state $f = \bar{f}_0$ (const.) becomes unstable. In order to obtain the transition point $c = c_{\text{tr}}$, we performed a linear stability analysis of the Boltzmann equation [32]. We add the perturbation $\delta f(\mathbf{r}, \theta, t)$ to ρ_0 , and define its Fourier component $\delta f_k(\mathbf{q})$ and the complex damping rate $\Lambda_k(\mathbf{q})$ via:

$$\delta f(\mathbf{r}, \theta, t) = \int d^2\mathbf{q} \sum_k \delta f_k(\mathbf{q}) e^{i(\mathbf{q}\cdot\mathbf{r} + k\theta)} e^{-\Lambda_k(\mathbf{q})t}, \quad (11)$$

where $k = 0, \pm 1, \pm 2, \dots$ is the index of the Fourier modes in the angular domain. From the stability analysis, we find that only the damping rate of the mode $k = \pm 1$ can become negative. Their damping rate is given by

$$\text{Re } \Lambda_{\pm 1}(\mathbf{q}) = s(1 - 2\pi p_1) - 4\sqrt{2}c\bar{\mathcal{I}}f_0 \left\{ \frac{2}{3}(2\pi\hat{p}_1) \left(1 + \hat{\mathcal{I}}(\mathbf{q}) \right) - 1 \right\}, \quad (12)$$

where p_1 and \hat{p}_1 are the Fourier components of $p(\theta)$ and $\hat{p}(\theta)$ for $k = 1$, respectively, and

$$\bar{\mathcal{I}}f_0 = \frac{1 - \exp\left(-\frac{\rho_0 R_D^2}{2} \left(\Phi + \frac{1}{\rho_0 R_0^2} \right)\right)}{\Phi + \frac{1}{\rho_0 R_0^2}} + \rho_0 R_D^2 \int_1^\infty d\xi \xi e^{-\frac{R_D^2}{2R_0^2} \xi^2} \left(e^{\frac{3}{2}\xi} e^{-2\xi} \right)^{\rho_0 \Phi R_D^2}. \quad (13)$$

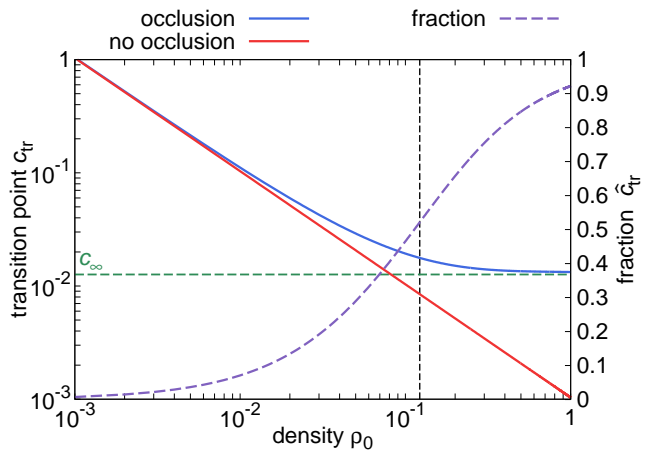


FIG. 2. The transition point c_{tr} as a function of the density ρ_0 . We set the biologically reasonable parameter values $s = 2$, $\kappa = 6$, $\hat{\kappa} = 20$, $\Phi = 7^\circ$, $R_0 = 10$ [16, 26, 27, 33, 34] which are rescaled by the diameter $D = 1$ body length and 1 sec [35]. The blue solid line shows c_{tr} (Eq. (14)), and reaches the horizontal green dashed line c_∞ in high density limit. Note that the theory is valid only for $\rho_0 \ll \Phi/D^2$, and the black dashed line marks $\rho_0 = \Phi/D^2$. The red solid line corresponds to the no occlusion case $c_{\text{tr}}|_{D=0}$. The purple dashed line is the fraction \hat{c}_{tr} to the right vertical axis.

is a function of the dimensionless quantities $\rho_0 R_D^2$, $\rho_0 R_0^2$, and Φ . In Eq. (12), the wavenumber-dependent function $\hat{\mathcal{I}}(\mathbf{q})$ satisfies $-1 < \hat{\mathcal{I}}(\mathbf{q}) \leq 1$, and has the single maximum $\hat{\mathcal{I}}(\mathbf{0}) = 1$. Thus the transition point is determined by $\text{Re } \Lambda_1(\mathbf{0}) = 0$. In the no-occlusion case obtained in the point particle limit $D = 0$, we get $\hat{\mathcal{I}}(\mathbf{q}) = e^{-q^2 R_0^2/2}$. In the linear stability analysis, we neglected the advection term in Eq.(1), which does not affect the transition point [21, 24, 32].

We then obtain the transition point

$$c_{\text{tr}} = \frac{s}{4\sqrt{2}\bar{\mathcal{I}}f_0} \frac{1 - 2\pi p_1}{\frac{4}{3}(2\pi\hat{p}_1) - 1} := \frac{c_0}{\bar{\mathcal{I}}f_0}, \quad (14)$$

where c_0 increases when s increases, or when κ or $\hat{\kappa}$ decreases, which means that the transition is hindered by the orientational noise. Note that $2\pi\hat{p}_1$ must be larger than $3/4$ such that $c_0 > 0$. As shown in Fig. 2, c_{tr} decreases as ρ_0 increases, which meets the expectation that a higher density of agents induces stronger alignment. Notably, in the high-density limit $\rho_0 \rightarrow \infty$, c_{tr} takes the non-zero value $c_\infty = c_0\Phi$ if $D > 0$. This value is determined only by the reorientation property (c_0) and the angle of resolution Φ , and does not depend on the details of the intrinsic factor. In particular, it is non-zero in the limit $R_0 \rightarrow \infty$, where the interaction decays only due to occlusion. In contrast, for $D = 0$, we obtain $c_{\text{tr}}|_{D=0} = c_0/(\rho_0 R_0^2)$, which vanishes in the high-density limit and also in the limit $R_0 \rightarrow \infty$. These results show that the non-zero value of c_∞ originates from occlusion by finite-sized particles, and that the point-particle case

is obtained as a singular limit.

In Fig. 2, we also show the fraction $\hat{c}_{\text{tr}} = (c_{\text{tr}} - c_{\text{tr}}|_{D=0})/c_{\text{tr}}$. As a function of the density, it shows a substantial increase before reaching the limit of validity of the model $\rho_0 = \Phi/D^2$, and then converges to unity as $\rho_0 \rightarrow \infty$.

Discussions.— We incorporated the non-local visual interaction to the Boltzmann equation as the effective pairwise interaction. Our model shows that the visual screening effect raises the transition threshold for the interaction rate c , which becomes non-zero even in the limits of high density or infinite range of the intrinsic interaction. This result is in stark contrast to those of the local-interaction models that assume point-like particles [21, 23]. In those models, the transition threshold was determined by hydrodynamic equations that are obtained by truncating the hierarchical equations for the angular Fourier modes $f_k(\mathbf{r}, t) = (2\pi)^{-1} \int_{-\pi}^{\pi} f(\mathbf{r}, \theta, t) e^{-ik\theta} d\theta$. Our results reproduce those of the previous models of polar particles with ferromagnetic interactions by taking the local limit $R_0 \rightarrow 0$ with cR_0^2 kept constant. In this limit, the interaction kernel $I_{\text{vis}}[f]$ converges to the delta function $\delta(\mathbf{r}' - \mathbf{r})$ [37], and the linear growth rate $-\text{Re } \Lambda_1(\mathbf{0})$ becomes identical to μ of Eq. (31) in Ref. [21].

The damping rate $\text{Re } \Lambda_1$ also contains the information of the kind of the disorder-order phase transition. In previous local interaction models, instability of the modes with $\mathbf{q} \neq \mathbf{0}$ induce phase coexistence in the form of traveling bands, which is the origin of the discontinuous transition [21]. Therefore, the transition is continuous if the $\mathbf{q} \neq \mathbf{0}$ modes are linearly stable at the transition point. This holds if the damping rate has no density-dependence, which is the case for metric-free interactions [22]. On the other hand, the transition becomes discontinuous if the damping rate depends on the density [22]. In our model, we have $\partial\Lambda_1/\partial\rho_0 \neq 0$ and thus our system shows a discontinuous transition [38]. The non-locality of the interaction does not affect the kind of the phase transition. This is reasonable if we consider that the Vicsek model [9] has a finite interaction range and shows a weakly discontinuous transition [11]. Active nematics with non-local repulsion also shows a discontinuous order-disorder transition [24].

Let us now consider the model's behavior above the transition point. The advection term in the Boltzmann equation (1) introduces couplings between f_k and $f_{k\pm 1}$ in the mode expansion, which introduces an infinite-dimensional matrix in the linear stability analysis. However, in our model, only the mode with $k = \pm 1$ is linearly unstable at the transition point in the non-advective limit ($v_0 = 0$). It means that there is a finite window of c above the transition point where the damping rate for $f_{k \neq \pm 1}$ remains positive. In this window, contributions to $f_{|k|>1}$ by the advective couplings are $\mathcal{O}(v_0^{|k|-1} f_{\pm 1})$, which we

can neglect compared to non-advective terms for sufficiently small values of v_0 . Thus we can use the damping rate $\Lambda_k(\mathbf{q})$ obtained in the non-advective limit ($v_0 = 0$).

In our model, the wavenumber-dependence of the damping rates comes through $\hat{I}(\mathbf{q})$ in Eq. (12). Since $\hat{I}(\mathbf{q})$ is a decreasing function of q and R_0 , only long-wavelength modes are destabilized in the vicinity of the transition point, and the unstable range of q gets narrower for a larger interaction range. In particular, when we consider a finite two-dimensional system with the periodic boundary condition, the wavenumber is discretized and there is a finite window of c above c_{tr} where only the $\mathbf{q} = \mathbf{0}$ mode becomes unstable. In this case, the transition becomes continuous and we can calculate the polar order parameter defined by $P = \left| \int_{-\pi}^{\pi} d\theta \mathbf{e}(\theta) \langle f(\mathbf{r}, \theta, t) \rangle \right| / \rho_0 = |\langle f_1 \rangle| / f_0$, where the brackets mean spatiotemporal and ensemble averages. By truncating the hierarchical equations for f_k , we obtain the scaling law $P = P_0(c_{\text{tr}})(c - c_{\text{tr}})^{1/2}$ [36]. As shown in Fig. S2, the prefactor $P_0(c_{\text{tr}})$ is larger for smaller c_{tr} , which corresponds to large ρ_0 and/or large $\hat{\kappa}$.

Finally, we compare our result with the behavior of real organisms, using the examples of fish in a shallow tank showing two-dimensional collective motion. A phase transition is observed for tilapia (*O. niloticus* L.) when number density increases above a threshold [39], which is agreement with our model. On the other hand, as the number density increases, golden shiner (*N. crysoleucas*) shows rotating state [40], and cichlid (*E. suratensis*) exhibits many oriented sub-clusters which is not aligned as a whole cluster [8]. Our visual model can be extended to reproduce a various patterns including the latter two cases. The emergence of a rotating state is facilitated by introducing the dead angle [41] and the wall [42], and considering three-dimensional motion [43]. The polar order is also disturbed by anisotropic attraction and repulsion [44], the change of speed by interaction [14, 18], and non-circular shapes of an agent [4]. The effects of these interesting extensions are the subject of future work.

Acknowledgement.— We acknowledge financial support by JSPS KAKENHI Grant No. 23KJ0171 to S.I. and support by a research environment of Tohoku University, Division for Interdisciplinary Advanced Research and Education to S.I.

* uchida@cmpt.phys.tohoku.ac.jp

- [1] T. Vicsek and A. Zafeiris, Phys. Rep. **517**, 71 (2012).
- [2] V. H. Sridhar, L. Li, D. Gorbonos, M. Nagy, B. R. Schell, T. Sorochkin, N. S. Gov, and I. D. Couzin, Proc. Natl. Acad. Sci. U.S.A. **118**, e2102157118 (2021).
- [3] A. Strandburg-Peshkin, C. R. Twomey, N. W. F. Bode, A. B. Kao, Y. Katz, C. C. Ioannou, S. B. Rosenthal, C. J. Torney, H. S. Wu, S. A. Levin, and I. D. Couzin, Curr. Biol. **23**, R709 (2013).

- [4] D. J. G. Pearce, A. M. Miller, G. Rowlands, and M. S. Turner, Proc. Natl. Acad. Sci. U.S.A. **111**, 10423 (2014).
- [5] M. Moussaïd, D. Helbing, and G. Theraulaz, Proc. Natl. Acad. Sci. U.S.A. **108**, 6884 (2011).
- [6] J. E. Herbert-Read, A. Perna, R. P. Mann, T. M. Schaerf, D. J. T. Sumpter, and A. J. W. Ward, Proc. Natl. Acad. Sci. U.S.A. **108**, 18726 (2011).
- [7] R. Dukas, Constraints on information processing and their effects on behavior, in *Cognitive Ecology: The Evolutionary Ecology of Information Processing and decision making* (University of Chicago Press, Chicago, 1998).
- [8] J. Jhawar, R. G. Morris, U. R. Amith-Kumar, M. D. Raj, T. Rogers, H. Rajendran, and V. Guttal, Nat. Phys. **16**, 488 (2020).
- [9] T. Vicsek, A. Czirók, E. Ben-Jacob, I. Cohen, and O. Shochet, Phys. Rev. Lett. **75**, 1226 (1995).
- [10] I.D. Couzin, J. Krause, R. James, G.D. Ruxton, and N.R. Franks, J. theor. Biol. **218**, 1 (2002).
- [11] H. Chaté, F. Ginelli, G. Grégoire, and F. Raynaud, Phys. Rev. E **77**, 046113 (2008).
- [12] B. H. Lemasson, J. J. Anderson, and R. A. Goodwin, J. Theor. Biol. **261**, 501 (2009).
- [13] H. Kunz and C. K. Hemelrijk, Appl. Anim. Behav. Sci. **138**, 142 (2012).
- [14] R. Bastien and P. A. Romanczuk, Sci. Adv. **6**, eaay0792 (2020).
- [15] D. Castro, F. Ruffier, and C. Eloy, Phys. Rev. Research **6**, 023016 (2024).
- [16] B. Collignon, A. Séguret, and J. Halloy, R. Soc. open sci. **3**, 150473 (2016).
- [17] D. Gorbonos, N. S. Gov, and I. D. Couzin, PRX Life **2**, 013008 (2024).
- [18] S. Ito and N. Uchida, PNAS Nexus **3**, pgae264 (2024).
- [19] J. Toner and Y. Tu, Phys. Rev. Lett. **75**, 4326 (1995).
- [20] J. Toner and Y. Tu, Phys. Rev. E **58**, 4828 (1998).
- [21] E. Bertin, M. Droz, and G. Grégoire, J. Phys. A: Math. Theor. **42**, 445001 (2009).
- [22] A. Peshkov, S. Ngo, E. Bertin, H. Chaté, and F. Ginelli, Phys. Rev. Lett. **109**, 098101 (2012).
- [23] E. Bertin, A. Baskaran, H. Chaté, and M. C. Marchetti, Phys. Rev. E **92**, 042141 (2015).
- [24] A. Patelli, I. Djafer-Cherif, I. S. Aranson, E. Bertin, and H. Chaté, Phys. Rev. Lett. **123**, 258001 (2019).
- [25] F. Thüroff, C. A. Weber, and E. Frey, Phys. Rev. X **4**, 041030 (2014).
- [26] D. Pita, B. A. Moore, L. P. Tyrrell, and E. Fernández-Juricic, PeerJ **3**, e1113 (2015).
- [27] D. S. Calovi, A. Litchinko, V. Lecheval, U. Lopez, A. P. Escudero, H. Chaté, C. Sire, and G. Theraulaz, PLOS Comput. Biol. **14**, e1005933 (2018).
- [28] We adopt the von Mises distribution to $p(\theta)$, $\hat{p}(\theta)$, but our results do not change qualitatively in the case of the usual probability distribution satisfying $0 < p_k$, $\hat{p}_k \leq 1/(2\pi)$. See Section IV. E of Supplementary Material.
- [29] See Section I. A of Supplementary Material for derivation of Eqs.(6),(8), and Section I. B of Supplementary Material for derivation of $\mathcal{D}(R)$.
- [30] See Fig. S1 for plots of the occlusion factor G for uniform density.
- [31] See Section II of Supplemental Material for justification of the functional forms of $B(R)$ and $K(\psi)$, and Section IV. G of Supplemental Material, where we also confirmed that an alternative form of $K(\psi)$ does not qualitatively change the results.
- [32] See Section IV of Supplemental Material for the calculation of the transition point.
- [33] R. Bainbridge, J. Exp. Biol. **35**, 109 (1958).
- [34] O. Akanyeti, J. Putney, Y. R. Yanagitsuru, G. V. Lauder, W. J. Stewart, and J. C. Liao, Proc. Natl. Acad. Sci. U. S. A. **114**, 13828 (2017).
- [35] See Section III of Supplemental Material for the details of parameter choice.
- [36] See Section V of Supplemental Material for derivation of the scaling law, and Eq. (S71) for the expression of $P_0(c_{tr})$.
- [37] See Section VI of Supplemental Material for the behavior of the model in the local limit $R_0 \rightarrow 0$.
- [38] However, recent studies suggest that even if $\text{Re } \Lambda_1$ has no density-dependence on the mean-field level, hydrodynamic noises can renormalize it and render the transition discontinuous: D. Martin *et al.*, Phys. Rev. Lett. **126**, 148001 (2021); D. Martin *et al.*, J. Stat. Mech. (2024) 084003.
- [39] Ch. Becco, N. Vandewalle, J. Delcourt, P. Poncin, Physica A **367**, 487 (2006).
- [40] K. Tunstrøm, Y. Katz, C. C. Ioannou, C. Huepe, and M. J. Lutz, I. D. Couzin, PLoS Comput. Biol. **9**, e1002915 (2013).
- [41] A. Costanzo and C. K. Hemelrijk, J. Phys. D: Appl. Phys. **51**, 134004 (2018).
- [42] J. Gautrais, C. Jost, M. Soria, A. Campo, S. Motsch, R. Fournier, S. Blanco, and G. Theraulaz, J. Math. Biol. **58**, 429 (2009).
- [43] S. Ito and N. Uchida, J. Phys. Soc. Jpn. **91**, 064806 (2022).
- [44] Y. Katz, K. Tunstrøm, C. C. Ioannou, C. Huepe, and I. D. Couzin, Proc. Natl. Acad. Sci. U.S.A. **108**, 18720 (2011).